Polym. Korea, Vol. 50, No. 4, pp. 560-571 (2026)
https://doi.org/10.7317/pk.2026.50.4.560
ISSN 2234-8077(Online)

수계 환경에서 고분해성 밀러블 폴리우레탄 복합체의 물성 및 분해 거동

Jianxiang Weng, Shikun Li, Changsheng He*, Yunxiang Bai, Zhiying Li, Hengyang Liu, Hehui Wang, Fangyuan Zheng**, Qi Jin***, Hongzhen Wang*, and Zaifeng Li†

School of Chemistry and Molecular Engineering, Qingdao University of Science and Technology
*School of Polymer Science and Engineering, Qingdao University of Science and Technology
**Sinopec (Beijing) Research Institute of Chemical Industry Co., Ltd./National Engineering Research Center for Synthesis of Novel Rubber and Plastic Materials
***Tongli Tyre Co., Ltd.

(2026년 3월 3일 접수, 2026년 5월 2일 수정, 2026년 5월 2일 채택)

Study on the Properties and Degradation Behavior of Deeply Degradable Millable Polyurethane Composites in Aqueous Medium

Jianxiang Weng, Shikun Li, Changsheng He*, Yunxiang Bai, Zhiying Li, Hengyang Liu, Hehui Wang, Fangyuan Zheng, Qi Jin***, Hongzhen Wang*, and Zaifeng Li†**

School of Chemistry and Molecular Engineering, Qingdao University of Science and Technology, Shandong Qingdao 266042, China
**School of Polymer Science and Engineering, Qingdao University of Science and Technology, Shandong Qingdao 266042, China*
***Sinopec (Beijing) Research Institute of Chemical Industry Co., Ltd./National Engineering Research Center for Synthesis of Novel Rubber and Plastic Materials, Beijing 102500, China*
****Tongli Tyre Co., Ltd. Shandong Jining 272100, China*

(Received March 3, 2026; Revised May 2, 2026; Accepted May 2, 2026)

Abstract: Development of downhole sealing tools undergoing deeply self-degradation following sealing operations in unconventional oil and gas extraction is becoming a big challenge. In practical engineering applications, materials must undergo complete disintegration into fine fragments or powder under hydrothermal conditions. The degradation products should be able to pass through a 4 × 4 mm mesh without external force. In this study, calcium oxide (CaO) composited water-degradation millable polyurethane (MPU) composites were prepared employing CaO as a degradation accelerator in the composite system. The degradation behavior of MPU composites in a hydrothermal environment at 100°C was systematically investigated. As demonstrated by scanning electron microscopy (SEM) and optical photographs, the presence of CaO exacerbated damage to the composite surface morphology. The degradation mechanism was elucidated at the molecular level using techniques such as Fourier-transform infrared spectroscopy (FTIR). At a loading of 20 phr CaO, the PU composites disintegrated into powder within 24 h, passing through a 4 × 4 mm mesh. The incorporation of CaO into MPU achieves deep degradability of polyurethane, providing modified insights and an experimental foundation for the development of high-performance, deeply degradable downhole tool sealants.

Keywords: deeply degradable, calcium oxide, degradation behavior, millable polyurethane, aqueous medium.

Introduction

Multi-stage Fracturing of Horizontal Wells is a pivotal production enhancement technique for developing unconventional oil and gas resources. However, its conventional operational workflow, which involves milling out and retrieving downhole tools, suffers from significant drawbacks, such as high energy consumption, extended operational cycles, and substantial cost.[1-3] To overcome these limitations, degradable downhole tools have emerged as a promising solution. These tools are designed to automatic degradation after fulfilling their mission, thereby eliminating the need for intervention milling, which results in

†To whom correspondence should be addressed.
lizfengphd@126.com, ORCID 0000-0003-2347-923X

reduced operational expenditure and improved efficiency.[4,5] Consequently, imparting degradability to sealing materials has become a major focus of contemporary research.[6-8]

Generally, conventional sealing materials are mostly made of rubber, however, they lack the ability to degrade deeply. The recent research mainly focuses on using microorganisms and enzymes to achieve the complete degradation of rubber.[9-11] Zhang *et al*.[12] developed a biodegradable poly (vinyl alcohol) (PVA) elastomer exhibiting excellent solvent barrier properties and high elasticity. Nevertheless, its degradation rate reached only 20% after 120 days of burial in natural soil. Cheng *et al*.[13] investigated the degradation of vulcanized natural rubber using a soil consortium enriched with specific bacterial communities (Enriched bacterial consortia-3, NRE3), revealing its significant potential. However, the process remained protracted, achieving only 33% degradation after four weeks. The degradation of rubber using microorganisms or enzymes requires a prolonged processing time and often fails to achieve complete degradation. In addition, these biological agents are not suitable for functioning in high temperature and high-pressure environment. Polyurethane (PU) is extensively utilized in sealing applications due to its highly tailorable molecular architecture and superior mechanical properties.[14-16] In particular, polyester-based PU, rich in ester groups, is prone to hydrolysis at elevated temperatures, which makes it an ideal candidate for designing fully degradable sealing materials in aqueous environments.[17-19] However, despite having the potential to be fully degradable, the hydrolysis rate of the aforementioned elastomers at ambient conditions is relatively slow.

CaO reacts with water to form calcium hydroxide, releasing hydroxide ions (OH^-) and creating a localized alkaline environment. The alkaline environment facilitates the hydrolysis of urethane bonds, generating amine compounds and carbon dioxide (CO_2). Subsequently, the liberated CO_2 reacts with calcium hydroxide to form calcium carbonate ($CaCO_3$). This continuous metathesis reaction effectively promotes the hydrolysis reaction of polyurethane, thereby enabling the rapid and complete degradation of the PU composite.[20-23]

In this study, CaO was incorporated into MPU to prepare deeply degradable MPU composites. The influence of CaO content on crosslinking characteristics, mechanical properties, phase separation and hydrothermal degradation behavior of MPU composites was systematically investigated. Degradation mechanism for the MPU composites in aqueous medium was revealed. This work aims to provide robust experimental data and theoretical insights for development of high-performance, fully degradable polyurethane sealing materials for degradable downhole tools.

Experimental

Materials. Polyester polyurethane (PU), Dongguan Huagong Fosu New Materials Co., Ltd., Dongguan, China.; Zinc oxide (ZnO), Sinopharm Chemical Reagent Co., Ltd., Shanghai, China.; Stearic acid (SA), Tianjin Bodi Chemical Co., Ltd., Tianjin, China.; Calcium oxide (CaO), Sinopharm Chemical Reagent Co., Ltd., Shanghai, China.; Dicumyl peroxide (DCP), Shanghai Fangruida Chemical Co., Ltd., Shanghai, China.; Triallyl isocyanate (TAIC), Shanghai Demao Chemical Co., Ltd., Shanghai, China.; Carbon black (N220/N550/N774/N990), Shanghai Cabot Chemical Co., Ltd., Shanghai, China.

Preparation of CaO Composited MPUs. The CaO composited MPUs were prepared using the following procedure. The raw materials, including MPU, ZnO, SA, CaO, mixed carbon black, DCP, and TAIC, were sequentially compounded on a two-roll mill (Model X(S)K-160, Shanghai Shuangyi Rubber & Plastic Machinery Co., Ltd.). The resulting compound was then aged at room temperature for 24 h. Subsequently, it was vulcanized using a plate vulcanizer (Model XLB-DQ, Qingdao Yadong Machinery Co., Ltd., China). The crosslinking was conducted at 170 °C under 15 MPa for a duration corresponding to the optimal curing time (t_{90}+3 min). The formulations of the prepared samples are listed in Table 1.

Characterization and Measurements. Crosslinking Characteristics: The crosslinking characteristics of the compounds were analyzed using a Moving Die Rheometer (MDR

Table 1. Formulation of CaO Composited MPUs (unit: phr)

Samples	ZnO	SA	Mixing CB	DCP	TAIC	CaO
1#	5	1	60	3	1	0
2#	5	1	60	3	1	5
3#	5	1	60	3	1	10
4#	5	1	60	3	1	15
5#	5	1	60	3	1	20

2000, Alpha Technologies, USA) at a test temperature of 170 °C.

Mechanical Properties Testing: The mechanical properties of the vulcanizates, including tensile strength, elongation at break, and 100% modulus, were tested according to GB/T 528-2009. Shore A hardness was measured following GB/T 531-1991. All tests were conducted at room temperature, repeated five times, and the average values were reported.

Dynamic Mechanical Analysis (DMA): The dynamic mechanical properties of the composites were analyzed using a DMA instrument. Tests were performed in tension mode over a temperature range of -60 to 60 °C, at a frequency of 10 Hz and a strain amplitude of 25%.

Thermal Stability (TGA) Testing: Thermogravimetric analysis (TGA) was conducted from 25 to 600 °C at a constant heating rate of 10 °C/min under a nitrogen atmosphere.

Degradation Behavior: Standard dumbbell specimens were prepared from the vulcanizates and immersed in a water bath containing deionized water at 100 °C. At predetermined time intervals, five specimens were retrieved, dried, and tested to monitor the rate of mass change and mechanical properties (e.g., tensile strength, elongation at break, hardness) as a function of immersion time.

Microscopic Morphology: The microscopic morphological changes of the millable polyurethane before and after hydrolysis were examined using Scanning electron microscopy (SEM).

Macroscopic Morphology: The macroscopic morphological changes of the millable polyurethane before and after hydrolysis were documented using digital photography.

Fourier Transform Infrared Spectroscopy (ATR-FTIR): FTIR spectra were recorded in Attenuated total reflectance (ATR) mode across a wavenumber range of 4000 to 500 cm^{-1} with a resolution of 4 cm^{-1}.

Proton Nuclear Magnetic Resonance Spectroscopy. ^1H NMR spectrum was recorded on a Bruker Avance 400 MHz spectrometer (Bruker, Billerica, MA, USA) using a standard zg30 pulse sequence. The sample was dissolved in $CDCl_3$, and the spectrum was acquired at 298.9 K with a spectral width of 8196.7 Hz, an acquisition time of 4.00 s, and a relaxation delay (D1) of 1.0 s. A total of 16 scans were accumulated. Chemical shifts were referenced to the residual solvent signal of $CDCl_3$ (δ 7.26 ppm). The FID was processed with an exponential line broadening of 0.30 Hz.

Matrix Assisted Laser Desorption Ionization Time of Flight Mass Spectrometry. MALDI-TOF MS analysis was carried out on a Bruker UltrafleXtreme instrument (355 nm Nd:YAG laser, 2000 Hz) in reflectron or linear mode. Acceleration voltage: 20 kV; lens voltage: 8.02 kV; pulsed extraction: 170 ns. Spectra were accumulated from 500 laser shots over 10 sample spots. α-Cyano-4-hydroxycinnamic acid (CHCA) (15 mg/mL) was used as matrix. External calibration was applied.

Results and Discussion

The Crosslinking Characteristics. The crosslinking of MPUs is achieved *via* DCP-initiated free radical reaction. Firstly, DCP decomposes to generate free radicals, which attack the MPU macromolecular chains to form macro-radicals. Subsequently, these radicals further attack TAIC, construct a dense crosslinked network and significantly increase the crosslinking density (Figure 1). The presence of CaO does not directly participate in the chemical cross-linking of the system; rather, it provides physical cross-linking sites, thereby increasing the cross-linking density and rendering the cross-linked network more compact.

The effect of calcium oxide content on the crosslinking characteristic parameters of MPU composites is presented in Table 2. The crosslinking characteristic parameters of MPU composites exhibited a consistent increasing trend as the CaO content increased. The reaction between zinc oxide (ZnO) and stearic acid (SA) forming zinc stearate ($ZnSt_2$) is beneficial to promote crosslinking during curing.[24-28] As CaO is easier to react with stearic acid, the aforementioned formation of zinc stearate ($ZnSt_2$) was inhibited, which leads to a delayed onset of crosslinking and a reduced rate of the crosslinking reaction. Therefore, with an increase in CaO content, both the scorch time (t_{10}) and optimal cure time (t_{90}) showed similar increasing trend. Meanwhile, M_L increases with increasing CaO concentration, because the CaO agglomeration at higher loadings may limit chain movement. M_H and the delta torque ($\Delta M = M_H - M_L$) increase with CaO loading. This is because CaO, as a rigid inorganic filler, does not directly participate in the chemical crosslinking reaction. Instead, it enhances the densification of the crosslinked network through physical effects. As shown in Table 2, as the CaO content increases from 0 to 20 phr, $M_H - M_L$ rises consistently from 36.25 dN·m to 78.01 dN·m, indicating a significant enhancement in effective crosslinking density.[29-31]

Mechanical Properties. The tensile strength, hardness, and strength at 100% elongation of MPU composites exhibit an increasing trend with the increase in calcium oxide content, as presented in Table 3. This is attributed to CaO as a rigid inorganic filler, which effectively restricts chain mobility and enhances the stiffness and the tensile strength of MPU composites.[32-36] In

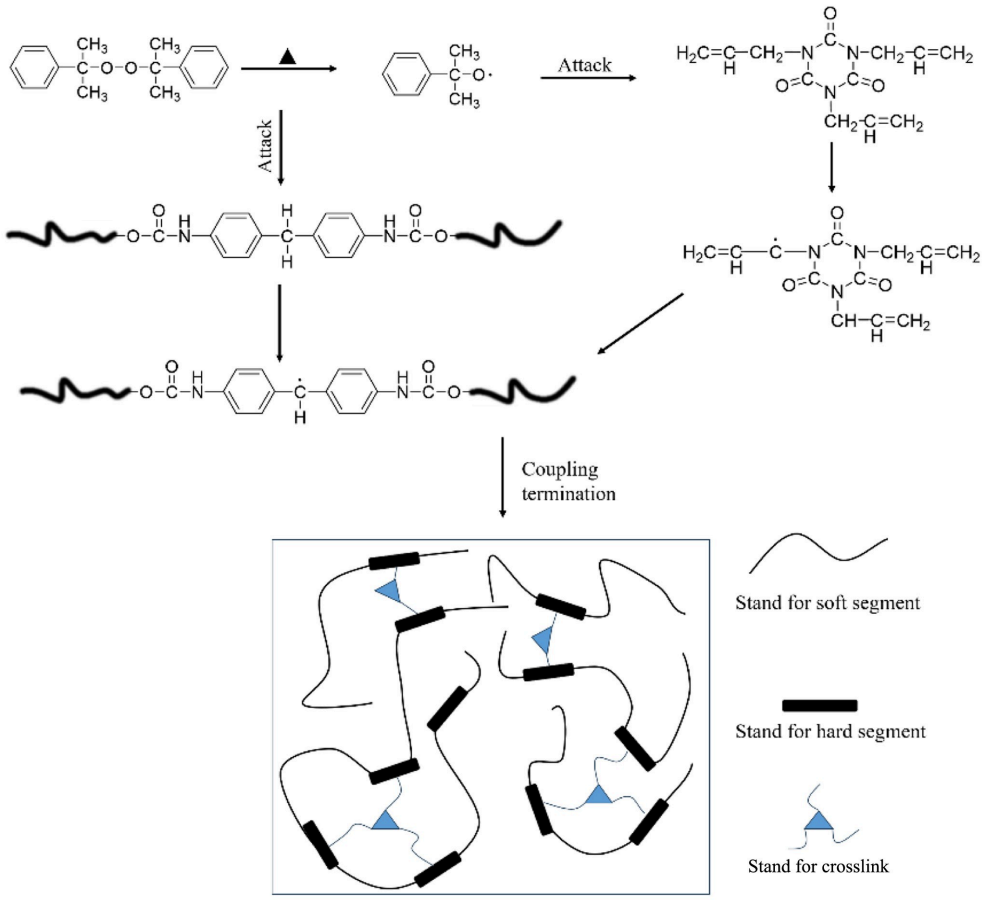

Figure 1. Cross-linking process of MPUs.

Table 2. Effect of CaO Content on the Crosslinking Characteristics Parameters of CaO Composited MPUs

Characterization parameters	Samples				
	1#	2#	3#	4#	5#
t_{10}/s	51	52	64	66	66
t_{90}/s	3638	4841	6037	6620	6626
M_L/dN·m	0.45	0.43	0.44	0.45	0.61
M_H/dN·m	36.7	55.48	65.85	74.54	78.62
M_H-M_L/dN·m	36.25	55.05	65.41	74.09	78.01

Notes: t_{10}, Scorch time; t_{90}, Optimum curing time; M_L, Minimum torque; M_H, Maximum torque; M_H-M_L, Delta torque

Table 3. Effect of CaO Content on the Mechanical Properties of CaO Composited MPUs

Properties	Formula				
	1#	2#	3#	4#	5#
σ/MPa	20.1	21.1	21.5	22.5	22.7
ε/%	214	130	123	113	93
100% σ/MPa	9.6	11.9	12.1	12.6	13.5
H/ Shore A	86	88	88	90	93

Notes: σ, tensile strength; ε, elongation at break; 100% σ, strength at 100% elongation; H, hardness

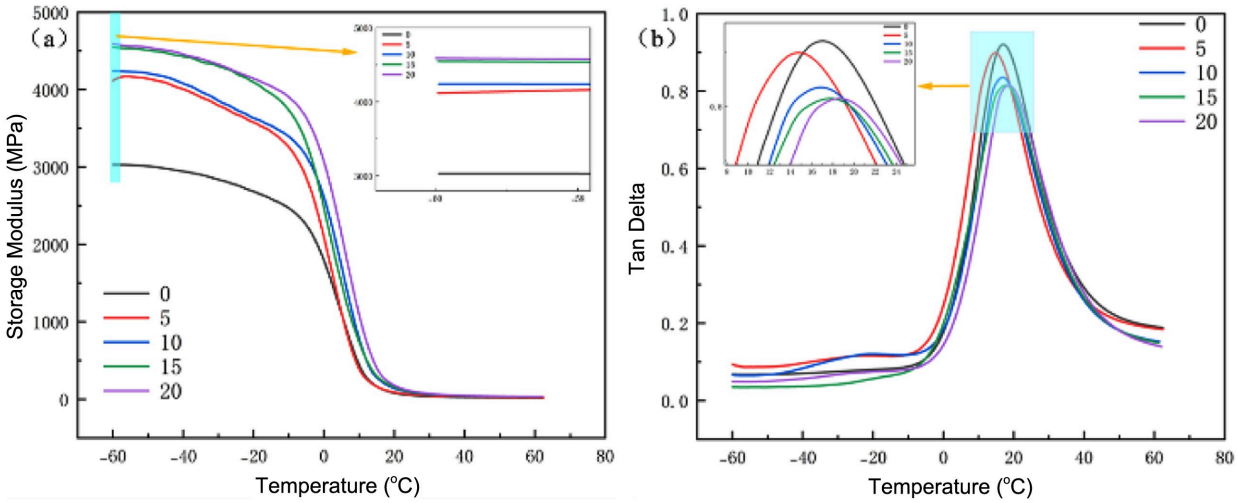

Figure 2. Dynamic mechanical properties of CaO composited MPUs with different calcium oxide contents: (a) Storage modulus; (b) Loss factor.

contrast, a consistent decline in elongation at break was observed with higher filler loading, primarily due to the restricted mobility of polymer chains caused by the reinforcing network formed by the rigid CaO, thereby enhancing stiffness but reducing flexibility and overall elongation capability. At higher CaO loadings, agglomeration becomes more pronounced, producing localized stress concentration sites that act as initiation points for crack propagation during deformation, thereby accelerating the fracture process of the material. To minimize the compromise of toughness while maintaining degradation performance, modification of CaO can be implemented, for instance, through surface modification using silane coupling agents or by employing nano-scale CaO to enhance dispersion.

Dynamic Mechanical Analysis. The inorganic rigid filler CaO continuously introduces physical cross-linking sites within the composite material. As illustrated by the variation in storage modulus shown in Figure 2(a), the storage modulus of the composite exhibits an upward trend with increasing CaO content and tends to plateau at higher concentrations. Furthermore, with an increase in CaO content, as shown in Figure 2(b) the loss factor (tan δ) of the composites exhibits an overall declining trend, while the glass transition temperature (T_g) shifts to higher values, because the incorporation of CaO facilitates microphase separation within the composite,[37] meanwhile CaO functioning as physical cross-linking sites. While an increase in cross-linking density enhances the rigidity of the MPU composite, it also imposes certain restrictions on the movement of the molecular chains.

Thermo-gravimetric Analysis. Figure 3 presents the thermogravimetric (TG) and derivative thermogravimetric (DTG)

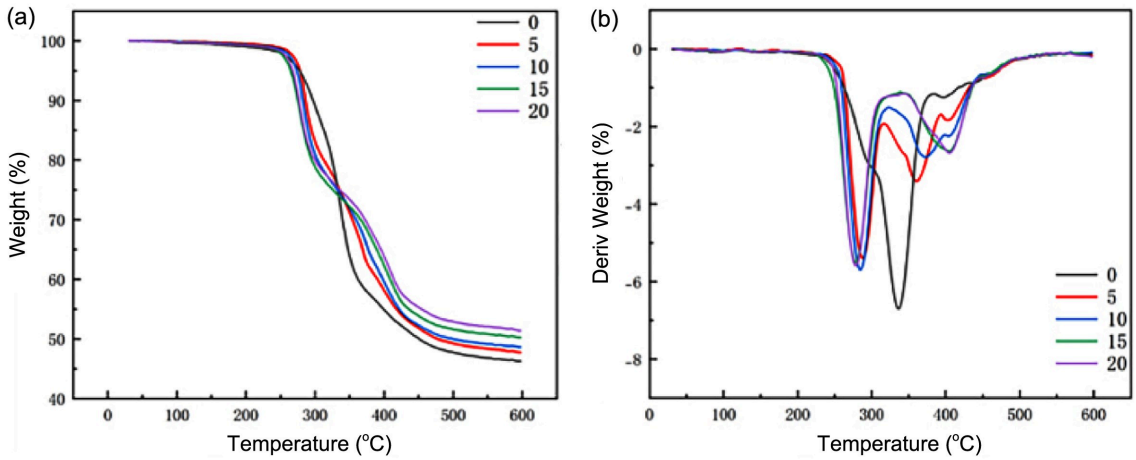

Figure 3. TG(a) and DTG(b) curves of CaO composited MPU.

curves of the MPU composites with varying CaO loadings. The incorporation of the CaO into the MPU composites leads to an obvious change in the TG curves under nitrogen atmosphere. The blank sample (Sample 1#) exhibits a single-stage pyrolysis in the TG curve, and one main decomposition peak occurring in the DTG curve around 330 °C, indicating an insignificant microphase separation in the MPU matrix. In contrast, all CaO composited MPUs showed two distinct weight loss stages, just like a typical phase-separated PU TG curve. The first stage (approximately 250-300 °C) corresponds to the thermal cracking of the polyurethane soft segment. The second stage (approximately 350-400 °C) corresponds to the thermal cracking of the polyurethane hard segment. The emergence of the second phase indicates that the incorporation of CaO promotes microphase separation, and with an increase in CaO content, the phenomenon of two distinct thermal degradation stages was more obvious.[37-39] It implied that stronger phase separation structure was got. It was speculated that CaO is an inorganic compound predominantly formed through ionic bonds. The calcium cation readily engages in strong interactions with the lone pair electrons on the nitrogen atom of the urethane linkage within the hard segments. This results in the adsorption of a substantial quantity of hard segments onto the CaO surface, thereby enhancing the microphase separation in the MPU. This interaction drives the MPU hard segments closer to the inorganic particle surface, thereby facilitating the aggregation of the hard segment phase.

Degradation Behavior. Degradation Behavior of CaO Composited MPUs: MPUs with CaO incorporated at 0, 5, 10, 15, and 20 phr were evaluated, the degradation behavior of samples with different CaO loading was shown in Figure 4. The blank control sample (without CaO) exhibited a cyclic degradation process under the aqueous medium at 100 °C, involving water ingress and hydrolysis, followed by dissolution and re-penetration. During this process, the mass of the composite material exhibits periodic fluctuations, and a certain correlation exists between these mass variations and changes in mechanical properties. Incorporation of the CaO into the MPU composites leads to a drastic change in the degradation behavior. The rate of change of mass increased, and the time to reach the maximum mass decreased with increasing CaO loading. This is attributed to the reaction of CaO with water to generate calcium hydroxide, which creates an alkaline environment. A higher CaO content results in a stronger alkalinity, which accelerates the hydrolysis of urethane bonds and consequently leads to rapid degradation of the composite. The changes in mechanical prop-

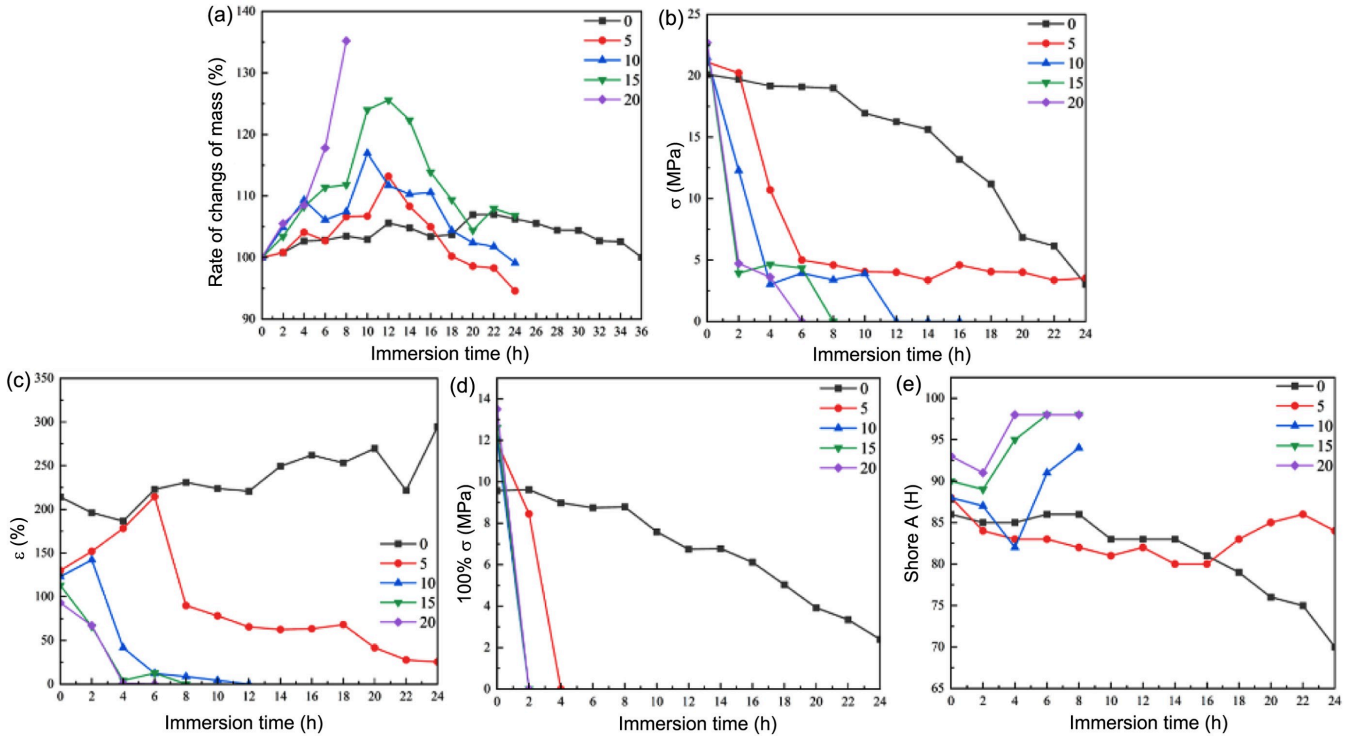

Figure 4. Degradation behavior of CaO composited MPUs with different calcium oxide loading in aqueous medium at 100 °C: (a) rate of change for mass; (b) tensile strength; (c) elongation at break; (d) strength at 100% elongation; (e) hardness.

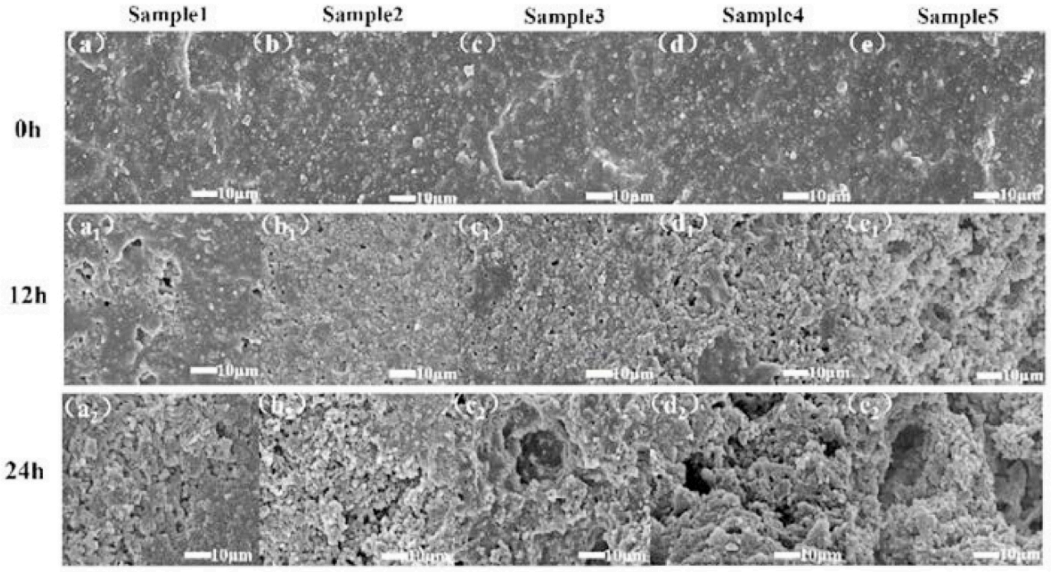

Figure 5. SEM images of MPU composites before and after degradation in an aqueous medium at 100 °C.

erties corroborated this acceleration effect. Compared with the blank control sample, the mechanical properties of MPU composites containing CaO exhibited a drastic decrease within a short time. For instance, the MPU composite with 20 phr CaO became too brittle for tensile testing after 6 hours, and then the sample deeply disintegrated into a powder after 12 h. At this moment, the aforementioned powder could pass through a 4×4 mm mesh with an efficiency exceeding 90% without external force (Figure 7). This indicates that the addition of calcium oxide enables the MPU composite material to achieve complete degradation through hydration and accelerated degradation.

Variation in Microscopic Morphology of CaO Composited MPUs. The evolution of microscopic morphology for MPU composites before and after hydrolytic degradation was observed by SEM. As demonstrated in Figure 5, a gradual increase in CaO agglomeration was observed in the initial state (0 h). After 12 h of immersion, all composites exhibited water-induced etching marks compared with the initial state. In addition, as the CaO loading increased, the aforementioned severity of etching escalated. After 24 h of immersion, the microscopic morphology of MPU composites with varying CaO contents exhibited obvious variations. Specifically, the etching marks of blank control sample occurred in localized areas. In contrast, as the CaO loading increased, the composites showed a large-area hydrolysis, which was manifested by an increase in the number of surface pores, diameter and depth, and then culminating in complete hydrolysis across the entire surface. This phenomenon can be attributed to CaO particles initially undergoing a hydration reaction at the interface zone. CaO particles react with water to generate calcium hydroxide with large particles, which subsequently facilitates the further penetration of water molecules into the composite interior. Meanwhile, the generated calcium hydroxide promotes the hydrolysis of urethane bonds, which leads to changes in the microscopic morphology of the MPU composites.

Variation in Macroscopic Shape of CaO Composited MPUs. Similarly, after 12 h of immersion, the blank control sample and the sample with low CaO content (5 phr) largely retained their initial shape. The composites with CaO content (5-15 phr) fractured, and the composite with CaO content (20 phr) was deeply comminuted into irregular fragments. After 24 h of immersion, the blank control sample and the sample with low CaO content (5 phr) were observed to maintain the dumbbell shape. The samples with CaO content (5-20 phr) exhibited more severe fragmentation, which were broken into a greater number of pieces.

MPU composites with 20 phr CaO after 24 h of hydrolysis were collected, dried, and then passed through a 4×4 mm filter. As illustrated in Figure 6, a large amount of grayish-white powder passing through the 4×4 mm sieve mesh was obtained. This phenomenon can be attributed to the following mechanism: the presence of CaO creates an alkaline environment, which accelerates the hydrolysis of the MPU composite. H_2O molecule attack urethane bonds and reacts with CaO to form $Ca(OH)_2$, and the CO_2 generated via decarboxylation is immobilized by the alkaline environment, leading to the formation of

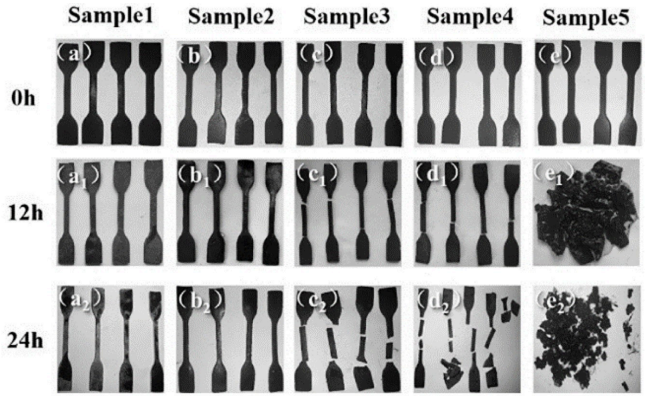

Figure 6. photograph of CaO composited MPUs before and after degradation in aqueous medium at 100 °C.

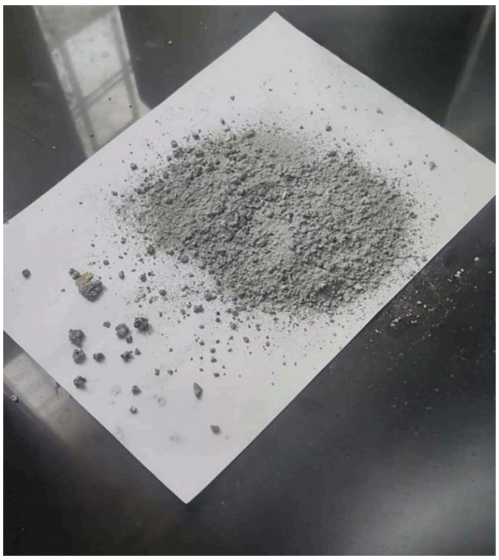

Figure 7. The shape of the 20 phr CaO MPU composite after sieving.

a small amount of calcium carbonate ($CaCO_3$). These processes collectively result in the final grayish-white powdered product. To verify the formation of the grayish-white powder containing inorganic mixture of CaO, $Ca(OH)_2$ and a small amount of $CaCO_3$, 5g hydrolysis product of the grayish-white powder was added to 18 g of a 36 wt% hydrochloric acid solution. After 12 h, the residue mixture weighed 3.56 g owing to the reactions of CaO, $Ca(OH)_2$ and a small amount of $CaCO_3$ with hydrochloric acid, at the same time, a few CO_2 bubbles escaping from solution were observed. These findings confirm that the grayish-white substance contains a small amount of $CaCO_3$ generated through hydrolysis, and further indicate that the addition of CaO promotes the hydrolysis of MPU by providing an alkaline environment, thereby achieving complete degradation of the material.

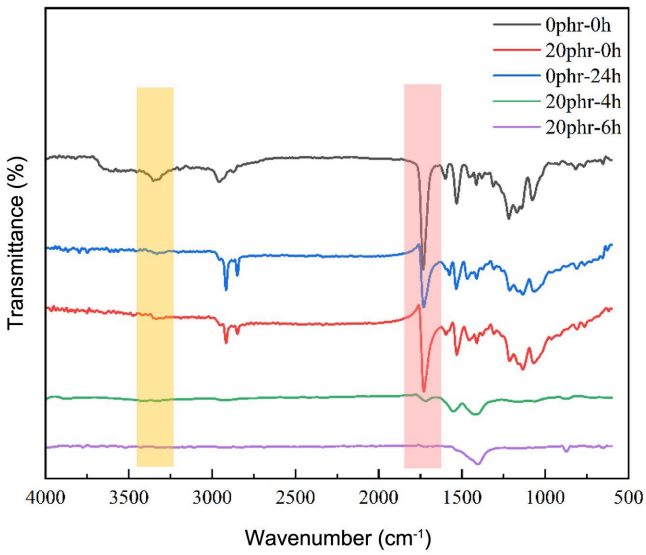

Figure 8. Infrared spectra of CaO composited MPUs and blank sample before and after immersion in an aqueous medium at 100 °C.

FTIR Spectra of CaO Composited MPUs Before and After Hydrolysis. The variation in macroscopic shape of MPU composites was explained by the hydrolysis of urethane bond, as shown in Figure 8. The absorption bands of MPU composites at 3430 cm^{-1} and 1730 cm^{-1} associated with urethane bonds were attributed to the stretching vibration of -NH groups and carbonyl groups (C=O), respectively. For unfilled MPU sample, the absorption intensity at 3430 cm^{-1} and 1730 cm^{-1} significantly decreased with prolonged degradation time, which is attributed to the hydrolysis of urethane bonds and ester bonds. Then, these generated products dissolved and diffused into aqueous medium. For MPU composite containing CaO of 20 phr loading, the absorption bands at 3430 cm^{-1} and 1730 cm^{-1} rapidly disappeared after 6 h, which indicated the addition of calcium oxide significantly accelerated the hydrolytic degradation of the MPU composite. The FTIR results help to understand the degradation behavior of MPU, and also demonstrate that the hydrolysis process of the MPU composites is manifested by the facilitated scission of urethane bonds and ester bonds by CaO degradation accelerator. Further analysis was conducted on the hydrolysis products of the modified MPU composite, and the results are presented in Figure 9.

As illustrated in Figure 9, the absorption band at 3474 cm^{-1} is attributed to the asymmetric stretching vibration of N-H groups, while the broad absorption band at 3315 cm^{-1} is attributed to stretching vibrations of alcoholic -OH. The absorption bands at 1699 cm^{-1} (C=O) and 1537 cm^{-1} (N-H bending) appeared, which further confirms the formation of amine species. The absorp-

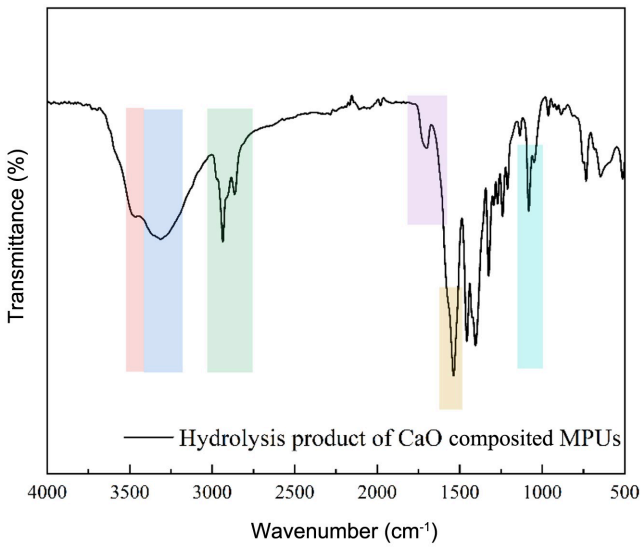

Figure 9. Infrared spectrum of hydrolysis products of CaO composited MPU.

tion band at 1404 cm^{-1} is attributed to the symmetric stretching vibration of carboxylate groups, and the stretching vibration bands of C-O (1081 cm^{-1} and 1135 cm^{-1}) provide strong evidence for the formation of alcohols *via* hydrolysis process. These results demonstrate that under alkaline hydrolysis conditions, the hydrolysis products of the modified MPU composite primarily consist of carboxylates, amines, and alcohols. The specific degradation mechanism is illustrated in Figure 10(II).

Proton Nuclear Magnetic Resonance Spectroscopy. Furthermore, we conducted ^{1}H NMR analysis to obtain detailed structural information. The ^{1}H NMR spectra of the original MPU and its hydrolysis products (Figure 11) reveal significant changes, providing direct evidence for the proposed bond cleavage mechanism. Specifically, for pristine MPU (red trace), characteristic signals corresponding to the polymer backbone and hard segment protons are observed in the downfield region (approximately δ 6.5-8.0 ppm for aromatic protons and δ 3.0-4.5 ppm for the urethane). In contrast, the spectrum of the hydrolysis products (blue trace) exhibits prominent new signals in the upfield region, particularly in the range of δ 1.0-2.5 ppm, which are characteristic of aliphatic protons adjacent to newly formed hydroxyl (-OH) and terminal amine ($-NH_2$) groups resulting from the hydrolysis of ester and urea/urethane bonds. Additionally, the relative intensities of the original polymer backbone signals have significantly diminished, while the signals corresponding to low-molecular-weight hydrolysis byproducts have emerged. This transformation confirms the extensive cleavage of the polymer chains and the generation of smaller, structurally defined degradation products, thereby validating the proposed degradation pathway.

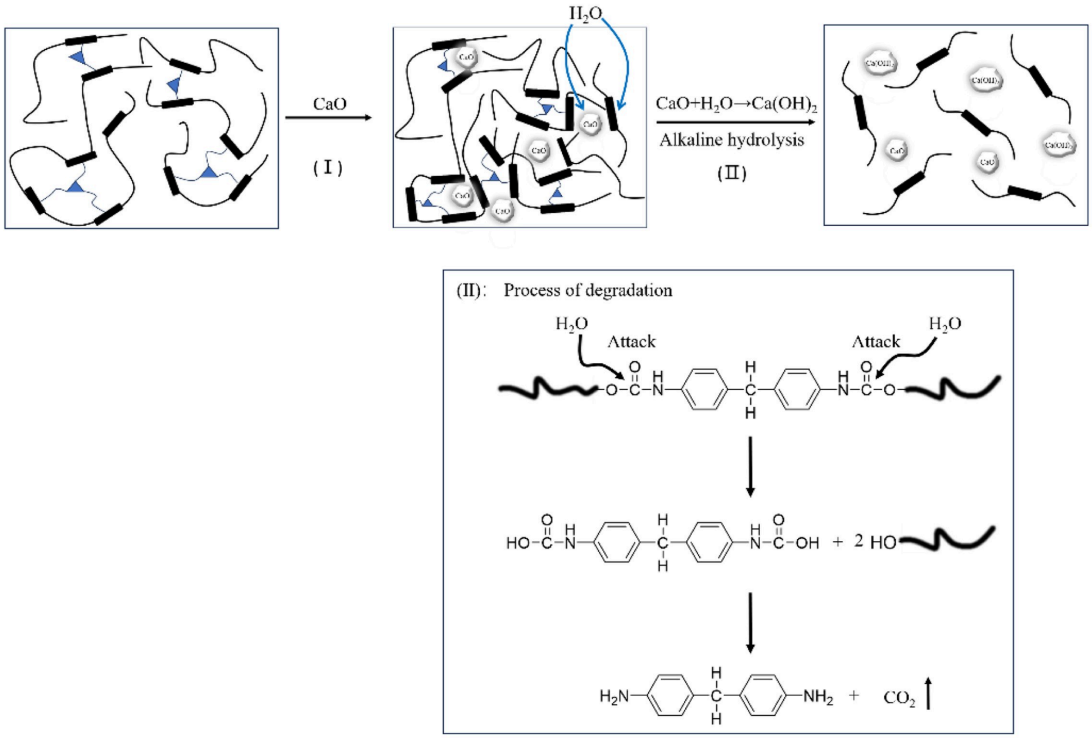

Figure 10. Degradation Mechanism of CaO composited MPU in Aqueous medium.

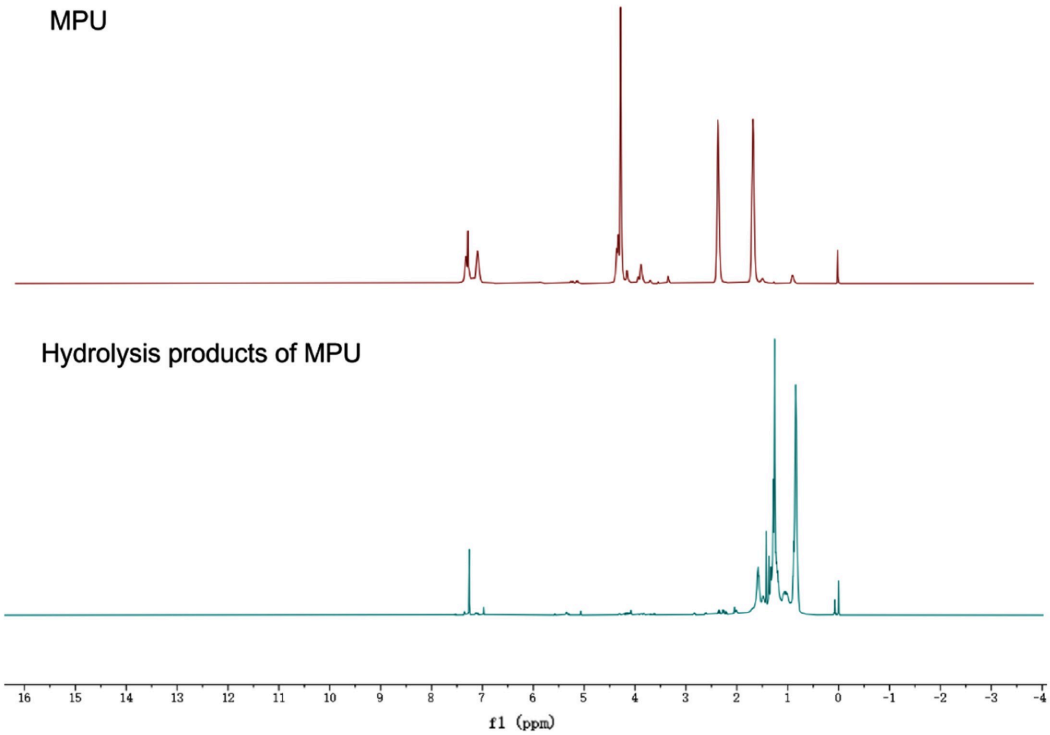

Figure 11. The NMR-H of hydrolysis products of MPU.

Matrix Assisted Laser Desorption Ionization Time of Flight Mass Spectrometry. The degradation product of the MPU composite containing 20 phr CaO after 24 h of hydrothermal treatment was analyzed by MALDI-TOF mass spectrometry (Figure 12). The spectrum reveals a series of intense peaks in the m/z range of 136-1772 Da, corresponding to oligomeric degradation products. The mass differences between consecutive peaks are approximately 200 Da, which matches the molecular weight of the repeating unit of the polyester soft segment. These results demonstrate that the MPU chains have undergone extensive hydrolytic scission, yielding low-molecular-weight oligomers. No peaks corresponding to high molecular weights (>5000 Da) were detected, confirming the completeness of degradation under the tested conditions. This MALDI-TOF analysis provides direct and conclusive evidence for the chain scission mechanism proposed in this work.

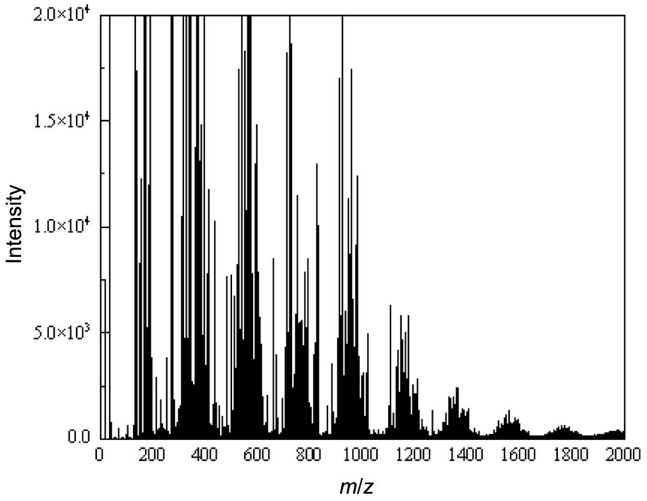

Figure 12. The MALDI-TOF of hydrolysis products of MPU.

Conclusions

In summary, a series of MPU composites were prepared by incorporating CaO as a degradation accelerator. CaO, as a rigid inorganic particle, played a physical crosslinking role in significantly enhancing the mechanical properties, which ensures the necessary rigidity and strength for downhole applications. Meanwhile, the physical crosslink interaction between CaO particles and polyurethane matrix markedly improved the crosslinking density of the MPU composites, thereby ensuring excellent sealing stability of the products under high-temperature and high-pressure conditions. The CaO unfilled MPU composite exhibited low degradation efficiency and failed to achieve complete degradation during the hydrothermal process. In contrast, the MPU composite at 20 phr CaO loading provided an alkaline

environment, which accelerated both the rate and degree of hydrolytic degradation for MPU composite. In particular, the CaO unfilled MPU composite still retained tensile strength of 2.62 MPa after 24 h of hydrolysis. While the MPU composite with CaO loading up to 20 phr lost its tensile strength in merely 10 h of hydrolysis. After 24 h, it deeply disintegrated into particles that could pass through a 4×4 mm mesh without external force, achieving complete degradation. FTIR data and other data indicated that the degradation mechanism of the MPU composites proceeded through the cleavage of urethane bonds and ester bonds. The degradation mechanism was further accelerated in an alkaline environment, which led to rapid and deep degradation of MPU composites. This study provides a novel insight and an experimental foundation for the development of high-performance, deeply degradable downhole tool sealants.

Acknowledgments: This work was financially supported by Advanced Materials-National Science and Technology Major Project (No.2026ZD0621600), National Natural Science Foundation of China (grant number, 22478215), Technological Innovation Guidance Program of Shandong Province (grant number, YDZX2025112), and Innovation leading Talent Project (grant number, tscx202408087).

Conflict of Interest: The authors declare that they have no known competing financial interests or personal relationships that could have appeared to influence the work reported in this paper.

References

1. Epelle, E. I.; Gerogiorgis, D. I. A Review of Technological Advances and Open Challenges for Oil and Gas Drilling Systems Engineering. *AIChE J.* **2020**, 66, e16842.
2. Hu, S.; Zhao, W.; Hou, L.; Yang, Z.; Zhu, R.; Wu, S.; Bai, B.; Jin, X. Development Potential and Technical Strategy of Continental Shale Oil in China. *Pet. Explor. Dev.* **2020**, 47, 877-887.
3. Teodoriu, C.; Bello, O. An Outlook of Drilling Technologies and Innovations: Present Status and Future Trends. *Energies* **2021**, 14, 4499.
4. Li, M.; Chen, L.; Wei, R.; Liao, C.; Fu, T. The Application of Fully Dissolvable Frac Plug Technique in Weiyuan Gasfield. SPE Kingdom of Saudi Arabia Annual Technical Symposium and Exhibition, Dammam, Saudi Arabia, 2018, April 23–26, SPE-192422-MS.
5. Yang, Y.; Cheng, Q.; Chen, J. Field Application of High-Temperature Dissolvable Bridge Plug in Shale Gas Horizontal Well. *J. Fail. Anal. Prev.* **2024**, 24, 1707-1718.
6. Fripp, M.; Walton, Z. Degradable Metal for Use in a Fully Dissolvable Frac Plug. *Offshore Technology Conference*, Houston, Texas, USA, 2016, May 2–5, D021S021R003.
7. Fripp, M.; Walton, Z.; Norman, T. Fully Dissolvable Fracturing Plug for Low-Temperature Wellbores. *SPE Annual Technical Conference and Exhibition*, San Antonio, Texas, USA, 2017, October 9–11, SPE-187335-MS.
8. Walton, Z.; Fripp, M.; Porter, J.; Vargus, G. Evolution of Frac Plug Technologies – Cast Iron to Composites to Dissolvable. *SPE Kingdom of Saudi Arabia Annual Technical Symposium and Exhibition*, Dammam, Saudi Arabia, 2018, April 23–26, SPE-194802-MS.
9. Ali Shah, A.; Hasan, F.; Shah, Z.; Kanwal, N.; Zeb, S. Biodegradation of Natural and Synthetic Rubbers: A Review. *Int. Biodeterior. Biodegradation* **2013**, 83, 145-157.
10. Boon, Z. H.; Teo, Y. Y.; Ang, D. T.-C. Recent Development of Biodegradable Synthetic Rubbers and Bio-based Rubbers Using Sustainable Materials From Biological Sources. *RSC Adv.* **2022**, 12, 34028-34052.
11. Shao, Y.; Mallory, R. C.; Dugas, M.; Flanagan, C.; Ligon, C.; Burks, G. R. Biodegradable Elastomers: Where Is the Solution? *Chem. Eur. J.* **2025**, 31, e202501440.
12. Zhang, N.; Pang, Y.; Li, Z.; Yang, C.; Zong, L.; Yang, H.; Wu, H.; Duan, Y.; Zhang, J. Rubber-like and Biodegradable Poly(vinyl alcohol) Composites with Triple Networks for High-efficiency Solvent Barrier. *Compos. Sci. Technol.* **2023**, 231, 109801.
13. Cheng, Y.; Wei, Y.; Wu, H.; Zhang, T.; Li, S.; Zhu, N.; Zhang, Q.; Li, W. Biodegradation of Vulcanized Natural Rubber by Enriched Bacterial Consortia. *Chem. Eng. J.* **2024**, 481, 148685.
14. Jiang, R.; Zheng, X.; Zhu, S.; Li, W.; Zhang, H.; Liu, Z.; Zhou, X. Recent Advances in Functional Polyurethane Chemistry: From Structural Design to Applications. *ChemistrySelect* **2023**, 8, e202204132.
15. Samokhvalova, S.; Lutz, J. F.; Coluzza, I. Precision Design of Sequence-Defined Polyurethanes: Exploring Controlled Folding Through Computational Design. *Macromol. Chem. Phys.* **2024**, 225, e202400223.
16. Zhang, J.; Yeoh, G. H.; Kabir, I. I. Polyurethane Materials for Fire Retardancy: Synthesis, Structure, Properties, and Applications. *Fire*. **2025**, 8, 64.
17. Hafeman, A. E.; Zienkiewicz, K. J.; Zachman, A. L.; Sung, H. J.; Nanney, L. B.; Davidson, J. M.; Guelcher, S. A. Characterization of the Degradation Mechanisms of Lysine-derived Aliphatic Poly(ester urethane) Scaffolds. *Biomaterials* **2011**, 32, 419-429.
18. Kotanen, S.; Poikelispää, M.; Efimov, A.; Harjunalanen, T.; Mills, C.; Laaksonen, T.; Sarlin, E. Hydrolytic Stability of Polyurethane/polyhydroxyurethane Hybrid Adhesives. *Int. J. Adhes. Adhes.* **2021**, 110, 102950.
19. Mondal, S.; Martin, D. Hydrolytic Degradation of Segmented Polyurethane Copolymers for Biomedical Applications. *Polym. Degrad. Stab.* **2012**, 97, 1553-1561.
20. Ramachandran, V. S.; Sereda, P. J.; Feldman, R. F. Mechanism of Hydration of Calcium Oxide. *Nature* **1964**, 201, 288-289.

21. Wan Isahak, W. N. R.; Che Ramli, Z. A.; Mohamed Hisham, M. W.; Yarmo, M. A. The Formation of a Series of Carbonates from Carbon Dioxide: Capturing and Utilisation. *Renewable Sustainable Energy Rev.* **2015**, 47, 93-106.
22. Dubina, E.; Korat, L.; Black, L.; Strupi-Šuput, J.; Plank, J. Influence of Water Vapour and Carbon Dioxide on Free Lime During Storage at 80 °C, Studied by Raman Spectroscopy. *Spectrochim. Acta Part A.* **2013**, 111, 299-303.
23. Glasson, D. R. Reactivity of Lime and Related Oxides. II. Sorption of Water Vapour on Calcium Oxide. *J. Appl. Chem.* **1958**, 8, 798-803.
24. Musto, P.; Larobina, D.; Cotugno, S.; Straffi, P.; Di Florio, G.; Mensitieri, G. Confocal Raman Imaging, FTIR Spectroscopy and Kinetic Modelling of the Zinc Oxide/stearic Acid Reaction in a Vulcanizing Rubber. *Polymer* **2013**, 54, 685-693.
25. Ikeda, Y.; Sakaki, Y.; Yasuda, Y.; Junkong, P.; Ohashi, T.; Miyaji, K.; Kobayashi, H. Roles of Dinuclear Bridging Bidentate Zinc/Stearate Complexes in Sulfur Cross-Linking of Isoprene Rubber. *Organometallics* **2019**, 38, 2363-2380.
26. Mostoni, S.; Milana, P.; D'Arienzo, M.; Dirè, S.; Callone, E.; Cepek, C.; Rubini, S.; Farooq, A.; Canevali, C.; Di Credico, B.; Scotti, R. Studying Stearic Acid Interaction with ZnO/SiO_2 Nanoparticles with Tailored Morphology and Surface Features: A Benchmark for Better Designing Efficient ZnO-based Curing Activators. *Ceram. Int.* **2023**, 49, 24312-24321.
27. Wang, H.; Xu, Q.; Liu, K.; Shi, B.; Zhang, L.; Tang, J.; Li, C.; Shen, J.; Jiang, H. Elucidation of the Reactive Process Involving ZnO Crystal Facets and Stearic Acid During Rubber Vulcanization. *Appl. Surface Sci.* **2025**, 710, 163889.
28. Ikeda, Y.; Yasuda, Y.; Ohashi, T.; Yokohama, H.; Minoda, S.; Kobayashi, H.; Honma, T. Dinuclear Bridging Bidentate Zinc/Stearate Complex in Sulfur Cross-Linking of Rubber. *Organometallics* **2015**, 48, 462-475.
29. Chen, L.; Guo, X.; Luo, Y.; Jia, Z.; Chen, Y.; Jia, D. Inorganic and Organic Hybrid Nanoparticles as Multifunctional Crosslinkers for Rubber Vulcanization with High-Filler Rubber Interaction. *Polymers* **2018**, 10, 1138.
30. Habeeb, S. A.; Alobad, Z. K.; Albozahid, M. A. The Effecting of Physical Properties of Inorganic Fillers on Swelling Rate of Rubber Compound: A review Study. *J. Univ. Babylon Eng. Sci.* **2019**, 27, 94-104.
31. Xu, Y.; Liu, Y.; Qin, X.; Liu, J.; Zhang, L. A Novel Strategy to Functionalize Styrene Butadiene Rubber Toward Enhanced Interfacial Interaction with Silica. *J. Appl. Polym. Sci.* **2023**, 140, e54476.
32. Lin, Y.; Liu, L.; Xu, G.; Zhang, D.; Guan, A.; Wu, G. Interfacial Interactions and Segmental Dynamics of Poly(vinyl acetate)/Silica Nanocomposites. *J. Phys. Chem. C* **2015**, 119, 12956-12966.
33. Park, G.; Lee, H.; Sim, J. H.; Kim, A.; Kim, M.; Paeng, K. Polymer Segmental Dynamics Near the Interface of Silica Particles in the Particle/polymer Composites. *J. Colloid Interface Sci.* **2023**, 629, 256-264.
34. Robertson, C. G.; Roland, C. M. Glass Transition and Interfacial Segmental Dynamics in Polymer-Particle Composites. *Rubber Chem. Technol.* **2008**, 81, 506-522.
35. Tanaka, K.; Tateishi, Y.; Okada, Y.; Nagamura, T.; Doi, M.; Morita, H. Interfacial Mobility of Polymers on Inorganic Solids. *J. Phys. Chem. B* **2009**, 113, 4571-4577.
36. Zhou, H.; Zha, H.; Zhang, Z.; Huang, J.; Liu, M. Advanced Mechanical Polymer Nanocomposites: from Confined Interphase to Structural Synergy. *Chem. Commun*. **2025**, 61, 16132-16149.
37. Yu, X.; Lv, Z.; Tong, Y.; Yang, R. The Effect of Inorganic Particles on Microphase Separation of Polyether Polyurethanes. *Polym. Mater. Sci. Eng.* **2013**, 29, 101-105.
38. Kalimullin, A. V.; Saprykina, N.; Zuev, V. V. The Effect of Type of Filler on Microphase Separation and Reinforcement in Polyurethane Based Composites. *J. Macromol. Sci. Part B: Phys.* **2021**, 60, 391-401.
39. Li, J.-W.; Tsen, W.-C.; Tsou, C.-H.; Suen, M.-C.; Chiu, C.-W.; Synthetic Environmentally Friendly Castor Oil Based-Polyurethane with Carbon Black as a Microphase Separation Promoter. *Polymers* **2019**, 11, 1333.